

SynthPix: A lightspeed PIV image generator

Antonio Terpin^{a,1,2}, Alan Bonomi^{a,2}, Francesco Banelli^a, Raffaello D’Andrea^a

^a*Institute for Dynamic Systems and Control, ETH Zürich, Zürich, Switzerland*

Abstract

We describe SynthPix, a synthetic image generator for Particle Image Velocimetry (PIV) with a focus on performance and parallelism on accelerators, implemented in JAX. SynthPix produces PIV image pairs from prescribed flow fields while exposing a configuration interface aligned with common PIV imaging and acquisition parameters (e.g., seeding density, particle image size, illumination nonuniformity, noise, blur, and timing). In contrast to offline dataset generation workflows, SynthPix is built to stream images on-the-fly directly into learning and benchmarking pipelines, enabling data-hungry methods and closed-loop procedures—such as adaptive sampling and acquisition/parameter co-design—without prohibitive storage and input-output costs. We demonstrate that SynthPix is compatible with a broad range of application scenarios, including controlled laboratory experiments and riverine image velocimetry, and supports rapid sweeps over nuisance factors for systematic robustness evaluation. SynthPix is a tool that supports the flow quantification community and in this paper we describe the main ideas behind the software package.

Keywords: Particle Image Velocimetry, PIV, synthetic image generation, fluid dynamics, deep learning, GPU acceleration

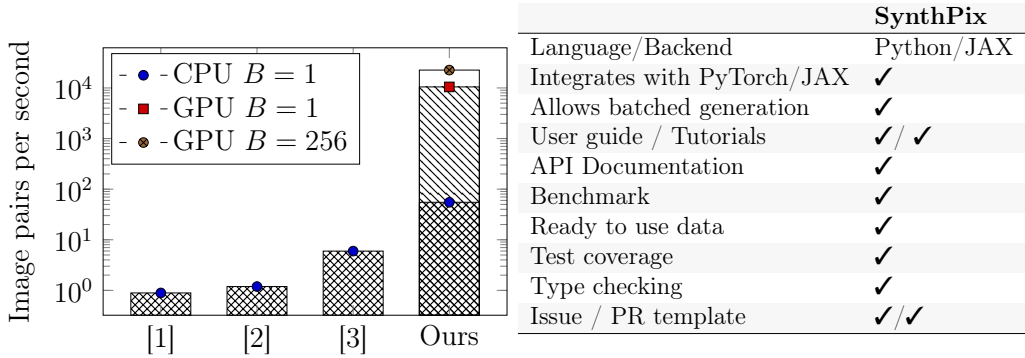
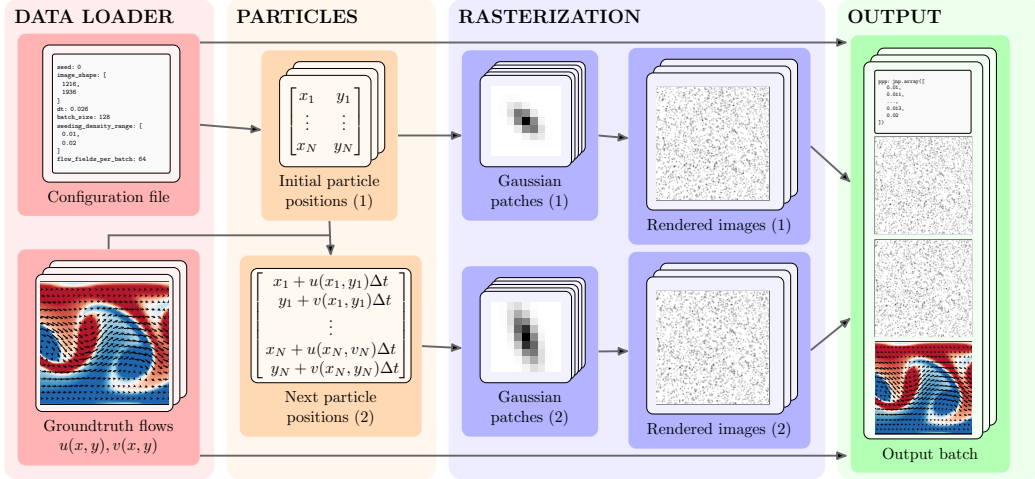
¹Corresponding author.

²Equal contribution.

Code metadata

Nr.	Code metadata description	Metadata
C1	Current code version	v0.1.0
C2	Permanent link to code/repository used for this code version	https://github.com/antonioterpin/synthpix
C3	Permanent link to Reproducible Capsule	https://github.com/antonioterpin/synthpix/blob/main/src/main.py
C4	Legal Code License	MIT License.
C5	Code versioning system used	git
C6	Software code languages, tools, and services used	Python
C7	Compilation requirements, operating environments & dependencies	Python 3.10+, Jax 0.6.2+, tqdm 4.67.1, h5py 3.13.0+, ruamel.yaml 0.18.10+, robo-goggles 0.1.7+
C8	If available Link to developer documentation/manual	https://github.com/antonioterpin/synthpix
C9	Support email for questions	aterpin@ethz.ch

Table 1: Code metadata



	SynthPix
Language/Backend	Python/JAX
Integrates with PyTorch/JAX	✓
Allows batched generation	✓
User guide / Tutorials	✓/ ✓
API Documentation	✓
Benchmark	✓
Ready to use data	✓
Test coverage	✓
Type checking	✓
Issue / PR template	✓/✓

Figure 1: The SynthPix pipeline (top) follows established PIV image-generation techniques but is optimized for performance on hardware accelerators. Below, we compare SynthPix’s throughput against existing synthetic particle-image generators (B: batch size; CPU/GPU: execution device) and summarize the key characteristics of the SynthPix codebase; see Section 3. The rendered images are zoomed in and white on black (instead of black on white) here and throughout the paper for visualization purposes.

1. Motivation and significance

Particle Image Velocimetry (PIV) [4–9] and related image-based flow-quantification methods [10–12] are among the central modalities for measuring flow fields across laboratory [5, 6], industrial [7, 13], microfluidic [14, 15], and environmental settings [16–19]. As application domains have broadened, so too have the underlying estimation methodologies. Correlation-based PIV remains the backbone of the field [20–24], while optical-flow-based methods provide an important complementary family of approaches [10–12, 25–27]. These applications are not limited to laboratory settings: similar image-based workflows arise in field deployments using bank-mounted, bridge-mounted, and airborne imaging platforms for natural flows, where LSPIV and STIV are established tools for non-intrusive surface-velocity estimation [16–19, 28].

Community benchmark efforts show that rigorous method comparison remains a central part of PIV methodology. The International PIV Challenge, in particular, helped standardize comparison on shared test cases with common evaluation procedures and reference solutions as a community practice [29–32]. Such benchmark datasets are highly valuable, but they are also necessarily finite and task-specific: they are assembled for particular modalities and operating conditions, and therefore cannot span the full range of particle densities, image diameters, noise levels, blur, illumination non-uniformities, displacement gradients, and out-of-plane losses that affect estimator behavior in practice. Synthetic generators make it possible to isolate, under reproducible conditions, the effects of particle image diameter, seeding density, noise, blur, illumination non-uniformity, displacement gradients, and out-of-plane loss, from early synthetic-image efforts for PIV assessment and benchmarking [29, 33, 34] to more recent benchmarking-oriented software and simulation frameworks [2, 35]. This role is important not only for controlled benchmarking, sensitivity analysis, uncertainty studies, and robustness evaluation, but also for learning-based PIV, where simple neural networks [36–38] have evolved into data-hungrier architectures [39–43].

However, offline dataset generation still does not cover the main workflows targeted by SynthPix because of scale and rigidity. Modern simulation collections already span multi-terabyte regimes before any PIV rendering, as illustrated by *The Well* (15 terabytes across 16 datasets) [44] and the *Johns Hopkins Turbulence Database* (well over 200 terabytes) [45]. Even using only 100 flow fields from such collections, together with five values each for seeding density, particle diameter, noise level, illumination level, and Δt , already yields hundreds of thousands of conditions. At 1024×1024 resolution, storing a single uint8 image pair for each condition already requires nearly one terabyte, and storing 100 pairs per condition requires tens of terabytes.

At that scale, generation, storage, transfer, and repeated reading during training become bottlenecks. Offline generation is also rigid: changing the flow source or rendering parameters requires regenerating samples, which is problematic for settings such as hard-example mining, robustness sweeps, and acquisition-parameter co-design that rely on an evolving sampling distribution.

Contributions. We present SynthPix, an open-source Python package for synthetic PIV image generation, implemented in JAX and designed for hardware accelerators and direct integration into learning and benchmarking pipelines. Unlike existing generators aimed primarily at offline image creation, SynthPix enables high-throughput batched generation on GPUs and streams images on-the-fly into downstream estimators and training loops. It retains the flexibility expected from established PIV generators, exposing physically meaningful imaging and acquisition parameters while supporting diverse flow-field sources through a unified interface. Empirically, SynthPix delivers image-pair throughput orders of magnitude beyond existing alternatives, making large-scale robustness studies and adaptive workflows practical. With documentation, tests, and an extensible design, it provides a reusable foundation for reproducible synthetic PIV data generation. See Figure 1 for an overview.

2. Software description

We developed SynthPix in parallel with related projects [46–49], which helped us design a flexible, easy-to-integrate data-generation pipeline. In this and the following section, we outline our main design choices; for a comprehensive explanation of the software and detailed tutorials, see Table 1.

Usage. Listing 1 shows the simple API we designed for SynthPix.

GPU enabled. The user can specify in the configuration file which device to use (e.g., “cpu”, “cuda:0”, or multiple GPUs).

Configuration file. The configuration file specifies all options SynthPix needs to generate synthetic PIV images. SynthPix allows the user to specify the image shape (e.g., 1024×1024), the batch size (e.g., $B = 256$), how many different flow fields to use for each batch (e.g., $F = 64$, so that $B/F = 256/64 = 4$ image pairs are generated from each flow field), and for how many consecutive batches a loaded flow field is reused (e.g., 1). SynthPix also provides several configurable generation and noise parameters.

```

# pip install synthpix
import synthpix

sampler = synthpix.make("/path/to/config.yaml")

batch = next(sampler)
images1 = batch.images1
images2 = batch.images2
flows = batch.flow_fields
params = batch.params

print(f"{images1.shape}")
print(f"{images2.shape}")
print(f"{flows.shape}")

# We can access the sampled generation parameters, for instance:
print(f"{params.seeding_densities.shape}")

# pseudo-code in a loop:
while my_cond:
    batch = next(sampler)
    images1 = batch.images1
    images2 = batch.images2
    flows = batch.flow_fields
    flows_estimated = my_estimator(images1, images2)
    print(f"EPE = {epe(flows_estimated, flows)}")

```

Listing 1: Using SynthPix to instantiate the image generator, get a new batch of PIV images, the corresponding ground-truth flows and the sampled parameters.

Data loaders and pre-fetching. SynthPix decouples image generation from the origin and storage format of the underlying flow field through a unified flow-provider interface. In practice, flow fields specified in the configuration are loaded and transferred to the target device for rendering, with optional pre-fetching to overlap data movement and computation.

The current implementation already supports several common representations, including `.hdf5` files from the Johns Hopkins Turbulence Database [50, 51], `.mat` files as in [52], and generic `.npy` arrays storing tuples of the form $(x, y, u(x, y), v(x, y))$. Existing PIV images can also be loaded alongside the flow field, enabling direct use of datasets that already provide paired images and velocities [39, 53]. More importantly, this interface is not tied to a fixed catalogue of datasets: flow fields may also be supplied procedu-

rally through a Python function, which makes it straightforward to integrate analytically defined or randomly generated flows [40, 54]. This includes, for example, web-accessible turbulence repositories and DNS databases for canonical turbulent flows [50, 51, 55], broader simulation libraries spanning multiple physical regimes and coupled PDE systems [44, 56], specialized CFD datasets for turbulent wakes and related engineering flows [57–59], and river-image-velocimetry frameworks and benchmark datasets for algorithm evaluation under realistic hydraulic and imaging conditions [18, 19, 60, 61].

Mathematical model for the contribution of the single particle. We model the contribution of the single particle to the pixel intensity $I(x, y)$ in the image as

$$I_0 \exp \left(-\frac{1}{2(1-\rho^2)} \left(\frac{(x-x_0)^2}{\sigma_x^2} - 2\rho \frac{(x-x_0)(y-y_0)}{\sigma_x \sigma_y} + \frac{(y-y_0)^2}{\sigma_y^2} \right) \right), \quad (1)$$

where I_0 is the peak intensity, (x_0, y_0) is the (continuous) particle position, and the parameters σ_x, σ_y, ρ determine the shape of the contribution. This is the classical model used for rendering synthetic PIV images, as presented in [7], with the difference that allowing $\rho > 0$ also permits axis-misaligned particles. All the parameters are sampled uniformly at random from a configurable interval for each particle in the first image. For the particles in the second image, we sample the variation of each parameter for each particle from a zero-mean Gaussian with specified variance.

Remark 2.1. A different approach for calculating I_0 , which we defer to future releases, is to consider the particles in three-dimensional space, apply a three-dimensional flow, and then compute $I_0(z) = q \exp \left(-\frac{1}{\sqrt{2\pi}} \left| \frac{2Z^2}{\Delta Z_0^2} \right|^s \right)$, where the particle scattering efficiency q , the thickness of the laser sheet ΔZ_0 , and the shape factor s are configurable parameters; see [7].

Remark 2.2. The current version assumes an orthogonal imaging geometry and a simplified sensor model. In particular, we do not yet model non-orthogonal projection effects [34] or detector-specific sampling properties such as finite pixel fill factor. We note that such effects depend on the sensing technology and imaging hardware, and should therefore not be interpreted as uniformly applying across camera types: for example, CCD- and CMOS-based systems differ in the extent to which these effects are relevant in practice. These imaging- and sensor-modeling extensions are deferred to future releases.

Finally, SynthPix-generated images are optionally adjusted according to a user-specified intensity histogram.

Sampling the particles. For the first image, we allocate particles according to the maximum configured particles-per-pixel value `ppp_max` and sample positions for $H \times W \times \text{ppp_max}$ candidate particles over the image domain. We then sample the actual `ppp` uniformly from the configured range and mask the excess particles by setting their intensities to zero. For the second image, we move the particles according to the mapping $(x, y) \mapsto (x + u(x, y), y + v(x, y))$, where (x, y) are the particle coordinates and $(u(\cdot, \cdot), v(\cdot, \cdot))$ are the flow field coordinates; see Figure 1.

Considerations on the aggregation of the particle contributions. We sum the contributions of all the particles to obtain the resulting image. This superposition is commonly adopted in the literature, and relies both on a low number of particles per pixel (`ppp`) and on the absence of interference phenomena [34]. Modeling these effects represents a meaningful extension of SynthPix and will be part of a future release. In the current version, to mitigate this, we allow the user to select a probability of hiding a particle from each image. That is, a particle may be rendered in the first image but not in the second, and vice versa. To exploit parallelism on accelerators with JAX, we keep the number of particles constant by setting the intensity of the hidden particles to zero.

Efficient rasterization. To efficiently sum the contributions of the particles, we first generate, in parallel, a batch of Gaussian kernels, one for each particle, with patch sizes of $3 \max(\{d_i\}) + 1$, where d_i are the diameters of the particles. These patches are generated according to the selected mathematical model for the single particles. Then, we sum these kernels to obtain the final image.

3. Illustrative examples

We compare SynthPix to existing alternatives and analyze its performance in different scenarios. The empirical data is collected on an Ubuntu 22.04 machine equipped with an AMD Ryzen Threadripper PRO 5995WX processor and four Nvidia RTX 4090 GPUs. The number of GPUs used and the exact experimental setup is detailed for each experiment below.

3.1. Comparisons to related software

There are several alternatives for synthetic PIV image generation; see, for instance, [1–3, 7, 34, 62]. However, the requirements of modern deep-learning approaches call for a pipeline with focus on parallelism on accelerators, compatible with existing machine learning infrastructure and that facilitates batched generation of large quantities of data. Moreover, to facilitate (i) the

	SynthPix	Synpivimage [1, 7]	PIV image gen. [2]	PIVlab [3, 62]
Language/Backend	Python/JAX	Python/Numpy	MATLAB	MATLAB
Integrates with PyTorch/JAX	✓	—	✗	✗
Allows batched generation	✓	✗	✗	✗
User guide / Tutorials	✓/ ✓	✓/ ✓	✓/ ✓	✓/ ✓
API Documentation	✓	✓	✗	✗
Benchmarks	✓	✗	✗	✗
Ready to use data	✓	✗	✓	✓
Test coverage	✓	✗	✗	✗
Issue / PR template	✓	✗	✗	✓

Table 2: Comparison of SynthPix to the available alternatives. Marks: ✓ means that the feature is deemed fully provided, ✗ if it is not, — if it is deemed possible with a (possibly inefficient) workaround.

sharing of algorithmic advancements, (ii) the benchmarking with the state-of-the-art, and (iii) the reproducibility of the proposed pipelines, we need an easy-to-install, easy-to-use, and easy-to-contribute-to software following open-source software engineering best practices. Existing methods do not satisfy these conditions: in fact, most existing work on deep-learning for fluid flow quantification uses their own dataset generator [38–41, 53, 63–65]. SynthPix has an edge over other packages in terms of usability, documentation, testing, and integrability with modern approaches; see Table 2. Moreover, its throughput vastly outperforms the existing alternatives.

3.1.1. Throughput

Experimental setup. We compare the throughput of each method by generating a number of 512×512 image pairs. Because the methods vastly differ in the generation speed and interface, we collect 100 image pairs for each baseline [1–3, 7, 62] and for our method, instead, 100’000. Moreover, since our method is the only one that is batched and can exploit a hardware accelerator, we collect data both on CPU and (a single, see Section 3.3 for an ablation on the number of GPUs) GPU and with batch sizes of 1 and 256.

Results. The results are on the bottom left of Figure 1. In every setting, SynthPix outperforms all other methods by orders of magnitude. In particular, the results show the benefit of exploiting hardware acceleration. We juxtapose two image pairs generated with PIVlab [3, 62] and SynthPix in Figure 2.

3.2. Quality of the generated images

We assess the quality of SynthPix-generated images through their usefulness for downstream PIV estimation. Across the following experiments, we compare estimator behavior on original data and on images generated with SynthPix to assess if the synthetic images preserve the information relevant

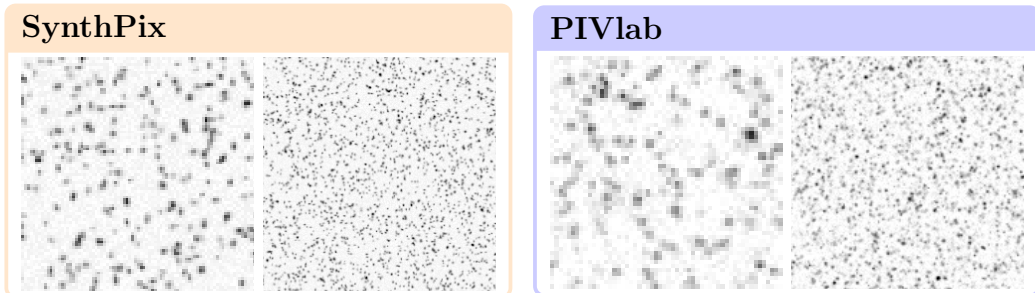


Figure 2: Zoomed-in images generated with SynthPix (left) and PIVlab [3] (right). For each method we report images of resolution 256×256 and 512×512 .

to benchmarking, analysis, and training. As the evaluation metric, we use the end-point error (EPE), defined as the mean pixelwise ℓ_2 distance between an estimated flow field and a reference flow field, averaged over the pixels (x, y) in the image domain I ,

$$\text{EPE}(u, v) := \frac{1}{|I|} \sum_{(x,y) \in I} \|u(x, y) - v(x, y)\|_2. \quad (2)$$

3.2.1. Estimator self-consistency on experimental PIV data

Experimental setup. We next consider experimental data from case A of the 2nd PIV Challenge [29]. Since no ground-truth flow is available for the experimental data, we assess re-rendering self-consistency. For each original image pair I_i^{orig} , we first estimate a flow field u_i with JPIV, generate a synthetic image pair I_i^{syn} from u_i using SynthPix, and then re-estimate the flow \tilde{u}_i from the synthetic images with JPIV. We report the average self-consistency error

$$\mathcal{C}_{\text{avg}} := \text{average}(\text{EPE}(\tilde{u}_i, u_i)) \quad \text{and} \quad \mathcal{C}_{\text{median}} := \text{median}(\text{EPE}(\tilde{u}_i, u_i)), \quad (3)$$

where average and median are taken over all the image pairs. Smaller values of $\mathcal{C}_{\text{avg}}, \mathcal{C}_{\text{median}}$ indicate that SynthPix better preserves the flow information recovered by the estimator from the original experimental data.

Results. The resulting self-consistency errors are $\mathcal{C}_{\text{avg}} = 0.536$ and $\mathcal{C}_{\text{median}} = 0.368$, indicating that re-estimating the flow from SynthPix-generated image pairs yields results close to those obtained from the original experimental images and is adequate for practical applications.

3.2.2. Benchmark-error prediction on synthetic reference data

Experimental setup. We use the synthetic PIV dataset [39, 53], which provides image pairs together with ground-truth flow fields. For each image pair, we

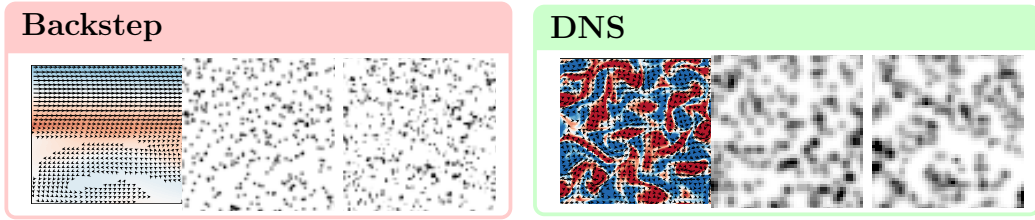


Figure 3: Flows (left), original (middle) and SynthPix-generated (right) images from two datasets of [39].

evaluate the DIS optical-flow estimator [26, 66] via Flow Gym [47] on both the original images and on corresponding images generated with SynthPix, and compare the resulting EPE values with respect to the same ground-truth flow field. To match the heterogeneous rendering conditions present in the original dataset, we tune the SynthPix generation parameters for each case to reproduce the visual characteristics of the corresponding reference images as closely as possible. To quantify how well evaluation on SynthPix predicts evaluation on the established benchmarks, we report the *relative EPE* (2) *discrepancy*

$$\mathcal{L}(u_1, u_2) := \frac{|\text{EPE}(u_1, \hat{u}) - \text{EPE}(u_2, \hat{u})|}{\text{EPE}(u_1, \hat{u})}, \quad (4)$$

where u_1 and u_2 denote the flows estimated from the original and SynthPix-generated images, respectively, and \hat{u} denotes the ground-truth flow. A value of $\mathcal{L}(u_1, u_2) = 0$ indicates that both evaluations yield identical EPE (2), while larger values indicate a larger deviation of SynthPix-based evaluation from the original benchmark.

Results. Over all image pairs, we obtain a relative discrepancy on the EPE of at most 0.005, averaging at 0.001, confirming the quality of the synthetic images generated with SynthPix. We also showcase, for different flow types in [39], a sample of images from [39] and from SynthPix in Figure 3.

3.2.3. Training learning-based estimators with SynthPix-generated data

Experimental setup. Finally, we evaluate SynthPix as a tool for generating training data for learning-based PIV estimation. We use flow fields derived from the PIV dataset to generate a substantially larger synthetic training set with SynthPix, train a RAFT-based estimator from Flow Gym [47] for three hours and fixed learning rate $\text{lr} = 0.0001$ on these generated image pairs, and test it on the original images. Performance is reported as the average EPE (2) on the original test set.

Results. Training on the enlarged SynthPix-generated dataset yields an average test EPE of 0.065 on the original images. Despite being trained on synthetic renderings rather than on the original images themselves, the model generalizes to the original test set with competitive accuracy, supporting the use of SynthPix for large-scale training data generation.

3.3. Ablations

In this section, we assess the performance impact of the generation parameters.

Experimental setup. We perform ablations on the number of GPUs, image size, seeding density, maximum particle diameter, minimum seeding density in the batch with fixed maximum, batch size, flow fields per batch, and batches generated with the same flow field. For each ablation study, we report the throughput in image pairs per second. The parameters that are not under study are fixed. In particular, we use a single GPU and consider an image size of 512×512 , a seeding density of 0.06, particle diameters sampled uniformly in $[0.8, 1.2]$, a batch size of 64, and 1 flow field per batch, kept for all the batches. The statistics are computed over 1000 batches.

Results. We collect the results in Figure 4 and make the following observations:

- The throughput scales linearly with increasing number of GPUs used, as one would expect from a software exploiting parallelism on accelerators.
- The throughput decreases with increasing image size, but remains high even for very large images, enabling the generation of high-resolution datasets.
- The throughput mildly decreases with increasing seeding density, approximately in a linear relationship. The throughput is not affected, instead, by the spread between the minimum and the maximum seeding density.
- The throughput decreases with increasing maximum particle diameter, but the trend resembles a staircase: the maximum particle diameter affects in discrete steps the Gaussian kernel patch size.
- The throughput increases substantially with the batch size initially, and then only mildly. This is not unexpected, since the increase in batch size amortizes the initial overheads of the accelerators, but these benefits are substantial only when moving from a single batch to multiple.
- The throughput is not affected by the number of flow fields used during generation, consistent with the parallelization over the flow fields.

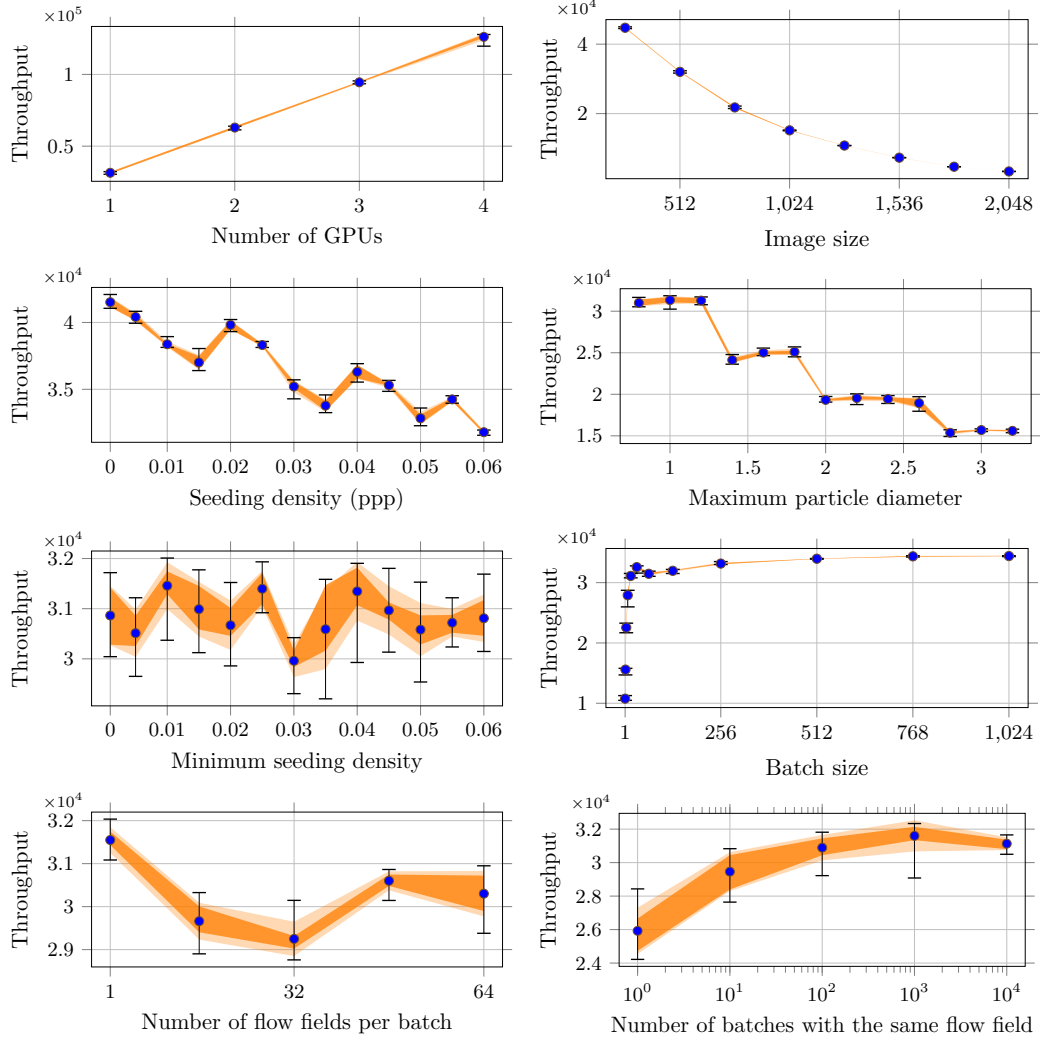


Figure 4: Results of the ablation studies in Section 3.3. Each plot shows how the throughput (in image pairs per second) changes with a single hyperparameter. The filled circles mark the mean over all the batches (we collect 1000 batches for each hyperparameter). The black vertical error bars extend between the minimum and maximum observed values. The orange bands represent the mean \pm one standard deviation (light) and the inter-quartile range (Q1–Q3, dark).

- The throughput increases only slightly with the number of batches with the same flow field. Future releases will load the data directly to the device.

4. Impact

SynthPix empowers researchers with a high-throughput pipeline to generate realistic and high-resolution PIV images compatible with modern deep-learning frameworks. SynthPix is written in JAX, enabling efficient large-scale training on hardware accelerators. With SynthPix, researchers can now push the limits of the use of synthetic data in the development of flow quantification methods and deploy more data-hungry algorithms. SynthPix has already supported multiple research works in adaptive PIV tuning [46], large-scale flow quantification [47], assessment of hard-constrained neural networks [49], and real-time feedback control [48]. Beyond these applications, SynthPix standardizes the generation of synthetic PIV datasets, removing the need for each study to “reinvent the wheel”. Its design and interoperability promote reproducibility and adoption across the machine-learning and fluid-dynamics communities, laying the foundation for new advances in data-driven flow quantification.

5. Conclusions

In this paper, we describe SynthPix, a synthetic image generator for PIV implemented in JAX, designed to maximize throughput via batching and parallelism on accelerators while retaining the configuration flexibility of established generators. Sections 3–4 show that SynthPix enables large-scale generation of high-resolution image pairs and supports workflows where data generation must keep pace with modern learning-based training and benchmarking pipelines. In the future, we plan to extend SynthPix by:

- Implementing the second approach for computing I_0 described in Remark 2.1 and non-orthogonal configurations for the camera model (see Remark 2.2)
- Enabling the synthesis of PIV images from multiple cameras in a volumetric setting, as needed for tomographic PIV and PTV pipelines [67].
- Reusing particle positions across consecutive frames, i.e., applying the flow for a second, possibly different, $\Delta t'$ to the “next particles positions” in Figure 1 to obtain the “initial particle positions” for the successive batch.

Ultimately, we will prioritize the needs of the community as expressed via open issues and pull requests.

Acknowledgement

The authors would like to acknowledge the editor and the anonymous reviewers for their valuable and constructive feedback. We believe that the review process substantially strengthened the manuscript and improved the presentation of our contribution.

References

- [1] M. Probst, synpivimage: A transparent way of generating synthetic particle image velocimetry (piv) images, gitHub release v1.0.0a6 (2024). URL <https://github.com/matthiasprobst/synpivimage>
- [2] L. Mendes, A. Bernardino, R. M. Ferreira, piv-image-generator: An image generating software package for planar PIV and Optical Flow benchmarking, *SoftwareX* 12 (2020) 100537. doi:10.1016/j.softx.2020.100537.
- [3] W. Thielicke, E. J. Stamhuis, PIVlab – Towards User-friendly, Affordable and Accurate Digital Particle Image Velocimetry in MATLAB, *Journal of Open Research Software* (2014). doi:10.5334/jors.bl.
- [4] I. Grant, Particle image velocimetry: A review, *Proceedings of the Institution of Mechanical Engineers, Part C: Journal of Mechanical Engineering Science* 211 (1) (1997) 55–76. doi:10.1243/0954406971521665.
- [5] R. J. Adrian, Particle-imaging techniques for experimental fluid mechanics, *Annual Review of Fluid Mechanics* 23 (1) (1991) 261–304. doi:10.1146/annurev.fl.23.010191.001401.
- [6] R. J. Adrian, J. Westerweel, Twenty years of particle image velocimetry, *Experiments in Fluids* 39 (2) (2005) 159–169. doi:10.1007/s00348-005-0991-7.
- [7] M. Raffel, C. E. Willert, F. Scarano, C. J. Kähler, S. T. Wereley, J. Kompenhans, *Particle Image Velocimetry: A Practical Guide*, Springer, 2018. doi:10.1007/978-3-319-68852-7.
- [8] J. Westerweel, G. E. Elsinga, R. J. Adrian, Particle Image Velocimetry for Complex and Turbulent Flows, *Annual Review of Fluid Mechanics* 45 (Volume 45, 2013) (2013) 409–436. doi:10.1146/annurev-fluid-120710-101204.

- [9] S. Scharnowski, C. J. Kähler, Particle image velocimetry – classical operating rules from today’s perspective, *Optics and Lasers in Engineering* 135 (2020) 106185. doi:10.1016/j.optlaseng.2020.106185.
- [10] T. Liu, L. Shen, Fluid flow and optical flow, *Journal of Fluid Mechanics* 614 (2008) 253–291. doi:10.1017/S0022112008003273.
- [11] T. Corpetti, D. Heitz, G. Arroyo, E. Mémin, A. Santa-Cruz, Fluid experimental flow estimation based on an optical-flow scheme, *Experiments in Fluids* 40 (1) (2006) 80–97. doi:10.1007/s00348-005-0048-y.
- [12] Q. Zhong, H. Yang, Z. Yin, An optical flow algorithm based on gradient constancy assumption for PIV image processing, *Measurement Science and Technology* 28 (5) (2017) 055208. doi:10.1088/1361-6501/aa6511.
- [13] C. Tropea, A. L. Yarin, J. F. Foss, et al., *Springer Handbook of Experimental Fluid Mechanics*, Vol. 1, Springer, 2007.
- [14] J. G. Santiago, S. T. Wereley, C. D. Meinhart, D. J. Beebe, R. J. Adrian, A particle image velocimetry system for microfluidics, *Experiments in Fluids* 25 (4) (1998) 316–319. doi:10.1007/s003480050235.
- [15] C. D. Meinhart, S. T. Wereley, J. G. Santiago, PIV measurements of a microchannel flow, *Experiments in Fluids* 27 (5) (1999) 414–419. doi:10.1007/s003480050366.
- [16] M. Muste, I. Fujita, A. Hauet, Large-scale particle image velocimetry for measurements in riverine environments, *Water Resources Research* 44 (4) (2008) W00D19. doi:10.1029/2008WR006950.
- [17] I. Fujita, H. Watanabe, R. Tsubaki, Development of a non-intrusive and efficient flow monitoring technique: The space-time image velocimetry (STIV), *International Journal of River Basin Management* 5 (2) (2007) 105–114. doi:10.1080/15715124.2007.9635310.
- [18] M. T. Perks, S. F. Dal Sasso, A. Hauet, E. Jamieson, J. Le Coz, S. Pearce, S. Peña-Haro, A. Pizarro, D. Strelnikova, F. Tauro, et al., Towards harmonisation of image velocimetry techniques for river surface velocity observations, *Earth System Science Data* 12 (2) (2020) 1545–1559. doi:10.5194/essd-12-1545-2020.
- [19] C. J. Legleiter, P. J. Kinzel, A framework to facilitate development and testing of image-based river velocimetry algorithms, *Earth Surface Processes and Landforms* 49 (4) (2024) 1361–1382. doi:https://doi.org/10.1002/esp.5772.

- [20] C. E. Willert, M. Gharib, Digital particle image velocimetry, *Experiments in Fluids* 10 (4) (1991) 181–193. doi:10.1007/bf00190388.
- [21] R. D. Keane, R. J. Adrian, Theory of cross-correlation analysis of PIV images, *Applied Scientific Research* 49 (3) (1992) 191–215. doi:10.1007/BF00384623.
- [22] F. Scarano, Iterative image deformation methods in PIV, *Measurement Science and Technology* 13 (1) (2001) R1. doi:10.1088/0957-0233/13/1/201.
- [23] H. Wang, G. He, S. Wang, Globally optimized cross-correlation for particle image velocimetry, *Experiments in Fluids* 61 (11) (2020) 228. doi:10.1007/s00348-020-03062-x.
- [24] Y. Lee, F. Gu, Z. Gong, D. Pan, W. Zeng, Surrogate-based cross-correlation for particle image velocimetry, *Physics of Fluids* 36 (8) (2024) 087157. doi:10.1063/5.0219706.
- [25] B. K. P. Horn, B. G. Schunck, Determining optical flow, *Artificial Intelligence* 17 (1) (1981) 185–203. doi:10.1016/0004-3702(81)90024-2.
- [26] T. Kroeger, R. Timofte, D. Dai, L. Van Gool, Fast Optical Flow Using Dense Inverse Search, in: B. Leibe, J. Matas, N. Sebe, M. Welling (Eds.), *Computer Vision – ECCV 2016*, Springer International Publishing, Cham, 2016, pp. 471–488. doi:10.1007/978-3-319-46493-0_29.
- [27] J. Pimienta, J.-L. Aider, Towards High-Speed And High-Resolution Real-Time Optical Flow Particle Image Velocimetry, *Proceedings of the International Symposium on the Application of Laser and Imaging Techniques to Fluid Mechanics* 21 (2024) 1–17. doi:10.55037/lxllaser.21st.74.
- [28] J. Le Coz, A. Hauet, P. E. Carbonneau, N. B. Melcher, R. Boursicaud, R. Le Boursicaud, G. Dramais, W. Brevis, et al., Performance of image-based velocimetry (LSPIV) applied to flash-flood discharge measurements in Mediterranean rivers, *Journal of Hydrology* 394 (1–2) (2010) 42–52. doi:10.1016/j.jhydrol.2010.05.049.
- [29] M. Stanislas, K. Okamoto, C. J. Kähler, Main results of the First International PIV Challenge, *Measurement Science and Technology* 14 (10) (2003) R63–R89. doi:10.1088/0957-0233/14/10/201.

- [30] M. Stanislas, K. Okamoto, C. J. Kähler, J. Westerweel, Main results of the second international PIV Challenge, *Experiments in Fluids* 39 (2) (2005) 170–191. doi:10.1007/s00348-005-0951-2.
- [31] M. Stanislas, K. Okamoto, C. J. Kähler, J. Westerweel, F. Scarano, Main results of the third international PIV Challenge, *Experiments in Fluids* 45 (1) (2008) 27–71. doi:10.1007/s00348-008-0462-z.
- [32] C. J. Kähler, T. Astarita, P. P. Vlachos, J. Sakakibara, R. Hain, S. Discetti, R. La Foy, C. Cierpka, Main results of the 4th International PIV Challenge, *Experiments in Fluids* 57 (6) (2016) 97. doi:10.1007/s00348-016-2173-1.
- [33] K. Okamoto, S. Nishio, T. Saga, T. Kobayashi, Standard images for particle-image velocimetry, *Measurement Science and Technology* 11 (6) (2000) 685–691. doi:10.1088/0957-0233/11/6/311.
- [34] B. Lecordier, J. Westerweel, The EUROPIV Synthetic Image Generator (S.I.G.), in: *Particle Image Velocimetry: Recent Improvements*, Springer Berlin Heidelberg, 2004, pp. 145–161. doi:10.1007/978-3-642-18795-7_11.
- [35] L. K. Rajendran, S. P. M. Bane, P. P. Vlachos, PIV/BOS synthetic image generation in variable density environments for error analysis and experiment design, *Measurement Science and Technology* 30 (8) (2019) 085302. doi:10.1088/1361-6501/ab1ca8.
- [36] Y. A. Hassan, O. G. Philip, A new artificial neural network tracking technique for particle image velocimetry, *Experiments in Fluids* 23 (1997) 145–154. doi:10.1007/s003480050096.
- [37] P.-H. Chen, J.-Y. Yen, J.-L. Chen, An Artificial Neural Network for Double Exposure PIV Image Analysis, *Experiments in Fluids* 24 (5–6) (1998) 373–374. doi:10.1007/s003480050185.
- [38] J. Rabault, J. Kolaas, A. Jensen, Performing particle image velocimetry using artificial neural networks: a proof-of-concept, *Measurement Science and Technology* 28 (12) (2017) 125301. doi:10.1088/1361-6501/aa8b87.
- [39] S. Cai, S. Zhou, C. Xu, Q. Gao, Dense motion estimation of particle images via a convolutional neural network, *Experiments in Fluids* 60 (4) (2019) 73. doi:10.1007/s00348-019-2717-2.

- [40] L. Manickathan, C. Mucignat, I. Lunati, Kinematic training of convolutional neural networks for particle image velocimetry, *Measurement Science and Technology* 33 (12) (2022) 124006. doi:10.1088/1361-6501/ac8fae.
- [41] C. Lagemann, K. Lagemann, S. Mukherjee, W. Schröder, Deep recurrent optical flow learning for particle image velocimetry data, *Nature Machine Intelligence* 3 (7) (2021) 641–651. doi:10.1038/s42256-021-00369-0.
- [42] Y. A. Reddy, J. Wahl, M. Sjö Dahl, Twins-PIVNet: Spatial attention-based deep learning framework for particle image velocimetry using Vision Transformer, *Ocean Engineering* 318 (2025) 120205. doi:10.1016/j.oceaneng.2024.120205.
- [43] Q. Zhu, J. Wang, J. Hu, J. Ai, Y. Lee, PIV-FlowDiffuser: Transfer-learning-based denoising diffusion models for particle image velocimetry, *Sensors* 25 (19) (2025). doi:10.3390/s25196077.
- [44] F. Agocs, M. Beneitez, M. Berger, B. Blancard, B. Burkhart, M. Cranmer, S. Dalziel, D. Fielding, D. Fortunato, J. Goldberg, K. Hirashima, S. Ho, Y.-F. Jiang, R. Kerswell, S. Maddu, M. McCabe, L. Meyer, J. Miller, R. Morel, P. Mukhopadhyay, S. Nixon, R. Ohana, L. Parker, F. Rozet, J. Shen, R. Watteaux, The Well: a Large-Scale Collection of Diverse Physics Simulations for Machine Learning, in: *Advances in Neural Information Processing Systems* 37, 2024, pp. 44989–45037. doi:10.52202/079017-1430.
- [45] E. Perlman, R. Burns, Y. Li, C. Meneveau, Data exploration of turbulence simulations using a database cluster, in: *Proceedings of the 2007 ACM/IEEE conference on Supercomputing*, ACM, 2007, pp. 1–11. doi:10.1145/1362622.1362654.
- [46] A. Bonomi, F. Banelli, A. Terpin, Particle image velocimetry refinement via consensus ADMM, *arXiv preprint arXiv:2512.11695* (2025). doi:10.48550/arXiv.2512.11695.
- [47] F. Banelli, A. Terpin, A. Bonomi, R. D’Andrea, Flow Gym, *arXiv preprint arXiv:2512.20642* (2025). doi:10.48550/arXiv.2512.20642.
- [48] A. Terpin, R. D’Andrea, Using reinforcement learning to probe the role of feedback in skill acquisition, *arXiv preprint arXiv:2512.08463* (2025). doi:10.48550/arXiv.2512.08463.

- [49] P. D. Grontas, A. Terpin, E. C. Balta, R. D’Andrea, J. Lygeros, Pinet: Optimizing hard-constrained neural networks with orthogonal projection layers, arXiv preprint arXiv:2508.10480 (2025). doi:10.48550/arXiv.2508.10480.
- [50] Y. Li, E. Perlman, M. Wan, Y. Yang, C. Meneveau, R. Burns, S. Chen, A. Szalay, G. Eyink, A public turbulence database cluster and applications to study lagrangian evolution of velocity increments in turbulence, *Journal of Turbulence* 9 (2008) N31. doi:10.1080/14685240802376389.
- [51] E. Perlman, R. Burns, Y. Li, C. Meneveau, Data exploration of turbulence simulations using a database cluster, in: *SC’07: Proceedings of the 2007 ACM/IEEE Conference on Supercomputing, 2007*, pp. 1–11. doi:10.1145/1362622.1362654.
- [52] G. R. Jassal, B. E. Schmidt, Synthetic particle image datasets for benchmarking PIV processing algorithms (2024). doi:10.17605/osf.io/cnk56.
- [53] L. Wei, X. Guo, Deep learning framework for velocity field reconstruction from low-cost particle image velocimetry measurements, *Physics of Fluids* 37 (1) (2025) 013629. doi:10.1063/5.0252483.
- [54] A. Smirnov, S. Shi, I. Celik, Random Flow Generation Technique for Large Eddy Simulations and Particle-Dynamics Modeling, *Journal of Fluids Engineering* 123 (2) (2001) 359–371. doi:10.1115/1.1369598.
- [55] J. Graham, K. Kanov, X. I. A. Yang, M. Lee, N. Malaya, C. C. Lalescu, R. Burns, G. Eyink, A. Szalay, R. D. Moser, C. Meneveau, A web services accessible database of turbulent channel flow and its use for testing a new integral wall model for LES, *Journal of Turbulence* 17 (2) (2016) 181–215. doi:10.1080/14685248.2015.1088656.
- [56] M. Takamoto, T. Praditia, R. Leiteritz, D. MacKinlay, F. Alesiani, D. Pflüger, M. Niepert, PDEBENCH: An Extensive Benchmark for Scientific Machine Learning, arXiv preprint arXiv:2210.07182 (2022). doi:10.48550/arXiv.2210.07182.
- [57] Z. Cooper-Baldock, P. E. Santos, R. S. A. Brinkworth, K. Sammut, WAKESET: A Large-Scale, High-Reynolds Number Flow Dataset for Machine Learning of Turbulent Wake Dynamics (2026). doi:10.57967/HF/7698.

- [58] A. Towne, S. T. M. Dawson, G. A. Brès, A. Lozano-Durán, T. Saxton-Fox, A. Parthasarathy, A. R. Jones, H. Biler, C.-A. Yeh, H. D. Patel, K. Taira, A Database for Reduced-Complexity Modeling of Fluid Flows, *AIAA Journal* 61 (7) (2023) 2867–2892. doi:10.2514/1.J062203.
- [59] Y. Luo, Y. Chen, Z. Zhang, CFDBench: A Large-Scale Benchmark for Machine Learning Methods in Fluid Dynamics, arXiv preprint arXiv:2310.05963 (2023). doi:10.48550/arXiv.2310.05963.
- [60] A. Patalano, C. M. García, A. Rodríguez, Rectification of Image Velocity Results (RIVeR): A simple and user-friendly toolbox for large scale water surface Particle Image Velocimetry (PIV) and Particle Tracking Velocimetry (PTV), *Computers & Geosciences* 109 (2017) 323–330. doi:10.1016/j.cageo.2017.07.009.
- [61] G. Bodart, J. Le Coz, M. Jodeau, A. Hauet, Synthetic River Flow Videos for Evaluating Image-Based Velocimetry Methods, *Water Resources Research* 58 (12) (2022) e2022WR032251. doi:10.1029/2022WR032251.
- [62] W. Thielicke, R. Sonntag, Particle Image Velocimetry for MATLAB: Accuracy and enhanced algorithms in PIVlab, *Journal of Open Research Software* 9 (1) (2021) 12. doi:10.5334/jors.334.
- [63] S. Cai, J. Liang, Q. Gao, C. Xu, R. Wei, Particle Image Velocimetry Based on a Deep Learning Motion Estimator, *IEEE Transactions on Instrumentation and Measurement* 69 (6) (2020) 3538–3554. doi:10.1109/tim.2019.2932649.
- [64] Q. Gao, H. Lin, H. Tu, H. Zhu, R. Wei, G. Zhang, X. Shao, A robust single-pixel particle image velocimetry based on fully convolutional networks with cross-correlation embedded, *Physics of Fluids* 33 (12) (2021) 127125. doi:10.1063/5.0077146.
- [65] Y. Lee, H. Yang, Z. Yin, PIV-DCNN: cascaded deep convolutional neural networks for particle image velocimetry, *Experiments in Fluids* 58 (12) (2017) 171. doi:10.1007/s00348-017-2456-1.
- [66] Z. Teed, J. Deng, RAFT: Recurrent All-Pairs Field Transforms for Optical Flow, in: A. Vedaldi, H. Bischof, T. Brox, J.-M. Frahm (Eds.), *Computer Vision – ECCV 2020*, Springer International Publishing, 2020, pp. 402–419.

- [67] D. Schanz, S. Gesemann, A. Schröder, Shake-The-Box: Lagrangian particle tracking at high particle image densities, *Experiments in Fluids* 57 (5) (2016) 70. doi:10.1007/s00348-016-2157-1.